Principal component analysis of the evolution of the Saharan air layer and dust transport: Comparisons between a model simulation and MODIS and AIRS retrievals

Sun Wong,[1] Peter R. Colarco,[2] and Andrew E. Dessler[1]

Received 18 January 2006; revised 18 April 2006; accepted 27 July 2006; published 31 October 2006.

[1] The onset and evolution of Saharan air layer (SAL) episodes during June–September 2002 are diagnosed by applying principal component analysis to the NCEP reanalysis temperature anomalies at 850 hPa, where the largest SAL-induced temperature anomalies are located along the west coast of Africa. The first principal component (PC) represents the onset of SAL episodes, which are associated with large warm anomalies located at the west coast of Africa. The second PC represents two opposite phases of the evolution of the SAL. The positive phase corresponds to the southwestward migration of the warm anomalies into the tropical-subtropical North Atlantic Ocean, and the negative phase corresponds to the northwestward migration into the subtropical to midlatitude North Atlantic Ocean and the southwest Europe. AIRS retrievals of temperatures in September 2002 verify the migration depicted by the second PC. In addition, a dust transport model (CARMA) and the MODIS retrievals of aerosol optical thickness are used to study the associated effects on dust distribution and deposition. The positive (negative) phase of the second PC corresponds to a strengthening (weakening) of the offshore flows in the lower troposphere around 10–20°N, causing more (less) dust being transported toward the tropical North Atlantic Ocean. The 700-hPa anticyclonic circulation associated with the warm anomalies plays a role in connecting the dust with the warm anomalies.

Citation: Wong, S., P. R. Colarco, and A. E. Dessler (2006), Principal component analysis of the evolution of the Saharan air layer and dust transport: Comparisons between a model simulation and MODIS and AIRS retrievals, *J. Geophys. Res.*, *111*, D20109, doi:10.1029/2006JD007093.

1. Introduction

[2] The Saharan air layer (SAL) is a well-mixed layer of dry, warm air located between the marine boundary layer and the ~500-hPa level [*Carlson and Prospero*, 1972]. From late spring to early fall, it is frequently advected westward with Saharan dust across the North Atlantic Ocean [*Carlson and Prospero*, 1972; *Prospero and Carlson*, 1972]. Recently, *Dunion and Velden* [2004] used the Geostationary Operational Environmental Satellite to track the SAL across the North Atlantic Ocean, finding a phenomenological connection between the SAL and the suppression of the tropical cyclone (TC) activity. They indicated that the dissipation of deep convection occurring in the interior of the SAL plays a role in suppressing the development of TC activity. Using satellite-derived aerosol optical thickness and cloud brightness temperature, *Wong and Dessler* [2005] verified the suppression of deep convection associated with the warm and dry anomalies of the SAL. A model that does not appropriately simulate the SAL will therefore tend to overestimate the intensity of TCs that are interacting with the SAL [*Dunion and Velden*, 2004]. Understanding the properties of the SAL and studying its evolution are therefore important tasks for numerical prediction of TCs.

[3] The SAL contains suspended Saharan dust [*Carlson and Prospero*, 1972; *Karyampudi et al.*, 1999; *Prospero and Carlson*, 1972], which propagates with the SAL. There have been many modeling studies that have investigated the large-scale intercontinental transport of dust. *Tegen and Miller* [1998], *Mahowald et al.* [2003], and *Colarco et al.* [2003] all demonstrated that the downwind dust distribution is mainly influenced by the dynamical transport rather than the magnitude of dust emission.

[4] The relationship between the meteorological (temperature and wind) and dust fields has also been studied previously. *Alpert et al.* [1998] showed that there is a spatial correlation between the assimilation temperature increments and dust concentrations in the eastern tropical North Atlantic Ocean. Assimilation temperature increments are defined as the temperature difference between the assimilated values and the general circulation model short-term forecast values. A model-simulated climatology by *Jones et al.* [2004] indicated that the westward transport of dust is modulated by African Easterly Waves, which propagate from the west coast of North Africa across the tropical Atlantic Ocean. *Karyampudi et al.* [1999] used lidar observations to show

[1]Department of Atmospheric Science, Texas A&M University, College Station, Texas, USA.
[2]NASA Goddard Space Flight Center, Greenbelt, Maryland, USA.

0148-0227/06/2006JD007093

detailed spatial relationships between Saharan dust plumes and the meteorological fields, with the maximum dust concentration located close to the midlevel African easterly jet. These studies all imply a coherency between the migration of the SAL and Saharan dust, and that the linkage between them is related to the propagation of African Easterly Waves.

[5] With the availability of data from the Moderate Resolution Imaging Spectroradiometer (MODIS) [*Kaufman et al.*, 1997; *King et al.*, 2003], sophisticated statistical analyses can be performed on global-scale satellite data to reveal new information about the interaction between large-scale meteorological fields and intercontinental dust transport. *Kaufman et al.* [2005] applied aerosol optical thickness (AOT) retrievals from MODIS to estimate the cross-Atlantic flux and deposition budgets of Saharan dust. They showed a high correlation during the summertime between the monthly averaged MODIS dust AOT and the magnitude of westward wind at 750 hPa near the tropical-subtropical west coast of Africa, verifying that dust amount transport from the African continent to the eastern North Atlantic Ocean is modulated by the offshore easterlies during summer.

[6] In this work, we study the evolution of the SAL and the associated dust transport and deposition over subseasonal timescales using both model simulations and measurements from the MODIS on board the Terra satellite. In the next section, we describe the dust transport model and the meteorological data used to drive the model. We also describe the satellite retrievals being used to evaluate the model results. In the third section, we apply statistical techniques to define two indices describing the onset and the evolution of each SAL episode that occurred from June to September in 2002. We identify different features related to the evolution of the SAL and the associated pattern of West African circulation. We also estimate the relative distribution of dust deposition between the eastern tropical North Atlantic and the region from northwest Africa to southwest Europe. Conclusions are presented in the last section.

2. Model and Data

2.1. Model Simulation

[7] Global dust distributions are simulated for the period June–September 2002 using the offline Community Aerosol and Radiation Model for Atmospheres (CARMA [*Toon et al.*, 1988; *Ackerman et al.*, 1995]), following a methodology similar to that used by *Colarco et al.* [2003]. The NCEP/NCAR reanalysis package [*Kalnay et al.*, 1996] and the NCAR Model for Atmospheric Transport and Chemistry (MATCH [*Rasch et al.*, 1997]) provide the meteorological fields (e.g., temperature fields, wind velocity fields, surface pressure, etc.) and physical parameterizations (e.g., clouds, convection) necessary to simulate the atmospheric state. Dust emissions were based on soil erodibility, soil wetness, and 10-m wind speeds [*Ginoux et al.*, 2001]. Dry deposition is the most important dust removal mechanism in terms of the total aerosol mass [e.g., *Ginoux et al.*, 2001], and is highly dependent on particle size, so to accurately simulate the evolution of the dust particle size distribution we distribute the dust over eight size bins between 0.1 and 10 μm radius and compute the fractional emissions for each bin. Dust emissions from our source scheme and atmospheric state from our MATCH run are archived every six hours over the simulation period. The horizontal spatial resolution of these fields and the subsequent dust simulations is approximately $1.875^\circ \times 1.875^\circ$ on a regular longitude and Gaussian latitude grid. The vertical grid is resolved in 28 sigma layers extending from the surface to approximately 35 km altitude; 18 of these layers are below 10 km altitude. These fields are read into CARMA, which merges the emissions and meteorological fields with the aerosol microphysical and transport continuity equation to simulate the full dust lifecycle. The time step in CARMA is 1800 s, so input meteorological fields are linearly interpolated to the model current time. Dust removal is represented in the model via three mechanisms: dry deposition, in- and below-cloud wet scavenging in large-scale cloud systems, and wet scavenging in convective updrafts [*Balkanski et al.*, 1993]. The dust AOT at 550 nm is computed for each model column from the CARMA column-integrated particle size distribution assuming Mie scattering and a refractive index of $1.50-0.01i$. Further details of the model and its validation are presented by *Colarco et al.* [2003].

2.2. Satellite Data

[8] The MODIS aerosol algorithm inverts the reflected solar radiance from six MODIS bands (0.55–2.1 μm) to retrieve daytime aerosol properties over cloud-free regions with 10-km resolution [*Kaufman et al.*, 1997; *Levy et al.*, 2003; *Remer et al.*, 2002]. Daily statistics of aerosol properties are calculated on grids of $1^\circ \times 1^\circ$ resolution and are archived in the MOD08 level-3 product (version 4) [*King et al.*, 2003]. We analyze here the 0.55-μm AOT product measured between June and September 2002. We use measurements made by the MODIS on board the Terra satellite, which crosses the tropical-subtropical Atlantic Ocean around 1200 UTC. In this paper, we focus on retrievals made over oceans only, where the retrieved AOTs are more reliable than those over lands [*Remer et al.*, 2002; *Kaufman et al.*, 2005].

[9] MODIS AOT includes radiance extinction from several types of aerosols. In the tropical and subtropical North Atlantic Ocean, the main contributors to AOT are from mineral dust, maritime aerosols (aerosols generated by sea spray), and aerosol from biomass burning in South Africa and the Sahel region. *Kaufman et al.* [2005] estimated the seasonal cycle of the relative contributions from these three types of aerosols to the total AOT. In the region of the tropical to subtropical North Atlantic Ocean, contributions from mineral dust to the total AOT is more than 50% in the summer and early autumn (June–September). The remaining contributors are mainly maritime aerosols. Since the CARMA simulation discussed in this paper includes only mineral dust, we would expect a difference at most of a factor of 2 between the MODIS and CARMA AOT (because dust contributes more than 50% of the total AOT in June–September).

[10] The warm temperature anomalies associated with the SAL obtained from the NCEP reanalysis can be compared to those obtained from the Atmospheric Infrared Sounder (AIRS) [*Strow et al.*, 2003; *Susskind et al.*, 1998] on board the Aqua satellite. AIRS measures upwelling infrared radiance in 2378 spectral channels and uses those measurements to provide accurate vertical profiles of atmospheric temperatures over cloud-free region at a horizontal resolution

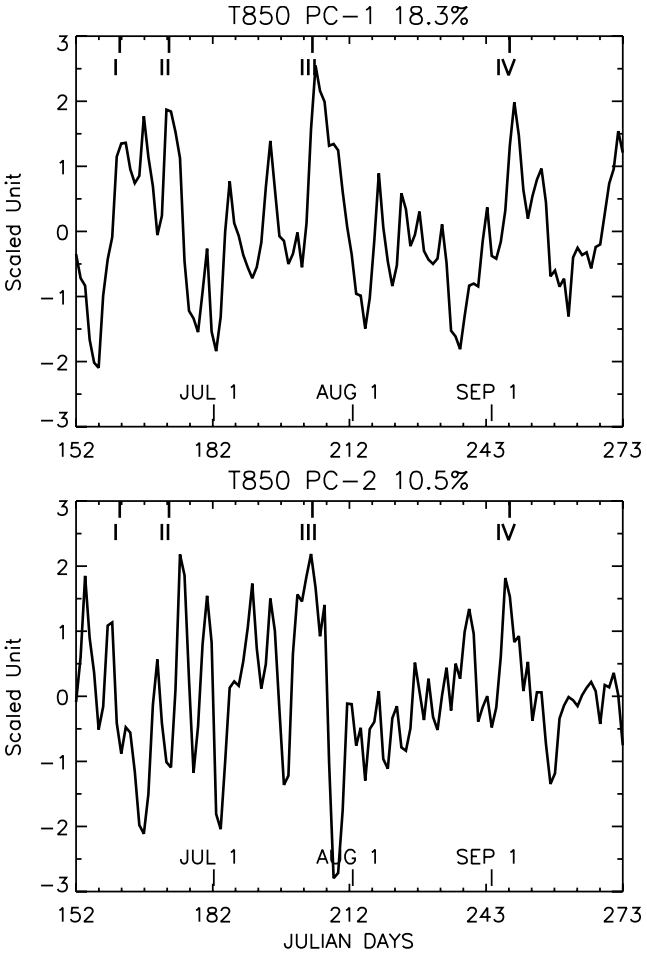

Figure 1. Time series of (top) the first and (bottom) the second principal components of the variation of 850 hPa NCEP reanalysis temperature anomalies for June–September 2002 over 0–40°N and 0–80°W. The abscissa is the Julian day number starting from 1 June 2002. The ordinate is scaled by the standard deviation of the time series (e.g., ±1 means at the ±1-σ levels). The contributions of the PCs to the total variability are also shown in the figure titles. The markers in Figure 1 (top) show the onset of the four main episodes being discussed in the text.

of ~50 km at nadir. The temperature retrievals are validated to 1 K in 1-km vertical layers over ocean [*Divakarla et al.*, 2006]. In this study, we use the daily level-3 product (version 3) with 1° × 1° spatial resolution to evaluate a SAL episode that occurred in early September 2002.

3. Results

3.1. Principal Components and Time Evolution

[11] We analyze the NCEP reanalysis temperature data at 850 hPa, where the warm anomalies associated with the SAL reach their maximum near the west coast of North Africa [*Wong and Dessler*, 2005]. Because of the rise in height of the base of the SAL and the cooling of the associated warm anomalies when the SAL moves westward across the Atlantic Ocean, we focus our analyses in the East and Central Atlantic Ocean, where the 850 hPa temperatures are a good proxy for the SAL. Temperature anomalies at 850 hPa are calculated for each day by subtracting the average 1200 UTC temperatures occurring over the period running from 15 days before to 15 days after the day of interest. Positive (negative) anomalies mean that the temperatures are higher (lower) than the seasonal values.

[12] We then apply principal component analysis (PCA [*Bretherton et al.*, 1992; *North et al.*, 1982; *Wong and Wang*, 2003]) to the temperature anomalies weighted by the grid area in the region of 0–80°W and 0–40°N, which covers the tropical to midlatitude North Atlantic Ocean and the west coast of North Africa. The time series and the patterns of the empirical orthogonal functions (EOFs) for the first two principal components (PCs) are shown in Figure 1 and Figure 2 (left). The first PC represents about 18% of the variability of temperature anomalies over the region, and the second PC represents about 11%. The errors of the eigenvalues are estimated by the rule stated by *North et al.* [1982]. The eigenvalues and the associated errors for the first, second, and third PCs are 6.67 ± 0.85, 3.82 ± 0.49, and 3.12 ± 0.40, respectively. Although the spread of the second and third PCs are marginally overlapped, the comparisons shown below between satellite AOT retrievals and CARMA dust simulation justify the physical reality of the second PC. Similar analysis using summertime NCEP temperatures for 1991–2005 (not shown) also gives similar pattern for the second PC. Years other than 2002 may illustrate interannual variation from the results shown in this study; however, the similarity between the empirical orthogonal functions (EOFs) of 2002 and of 1991–2005 in the eastern Atlantic Ocean justifies our choice of the year 2002, when MODIS and AIRS data are also available.

[13] We also analyze the NCEP wind velocity fields and the distributions of dust AOT from the model associated with the two PCs. The altitude at which the winds are most correlated with the transport of Saharan dust out of the African coast is about 700 hPa [*Kaufman et al.*, 2005]; therefore we analyze the NCEP winds at 700 hPa. We estimate the anomalies of the winds (and dust AOT) at each grid using the same method as was used for temperature. The wind anomalies reflect the subseasonal variations from the seasonal values. Positive (negative) AOT anomalies mean that the concentrations of dust are higher (lower) than the seasonal values. The dust AOT and winds anomalies are then regressed against the time series of the two PCs, in order to illustrate how the dust concentrations and the winds are associated with the temperature anomalies. The results are shown in Figure 2 (right).

[14] The first EOF (EOF-1, Figure 2, top left) shows large warm anomalies located off the west coast of Africa. The warm anomalies are centered at about 30°N and extend toward Europe as well as into the tropical-subtropical North Atlantic Ocean. The regression of the dust AOT anomalies on the first PC (Figure 2, top right) is spatially well correlated with the pattern of EOF-1. However, the maximum of dust AOT anomalies is located slightly to the south of the warm anomalies and coincides with the location of strong offshore wind anomalies. The strong offshore wind anomalies are related to the strong gradient of temperature anomalies by the thermal wind relation. Previous lidar measurements also show that dust anomalies tend to be close to the location of midlevel easterly jet [*Karyampudi et al.*, 1999]. In the

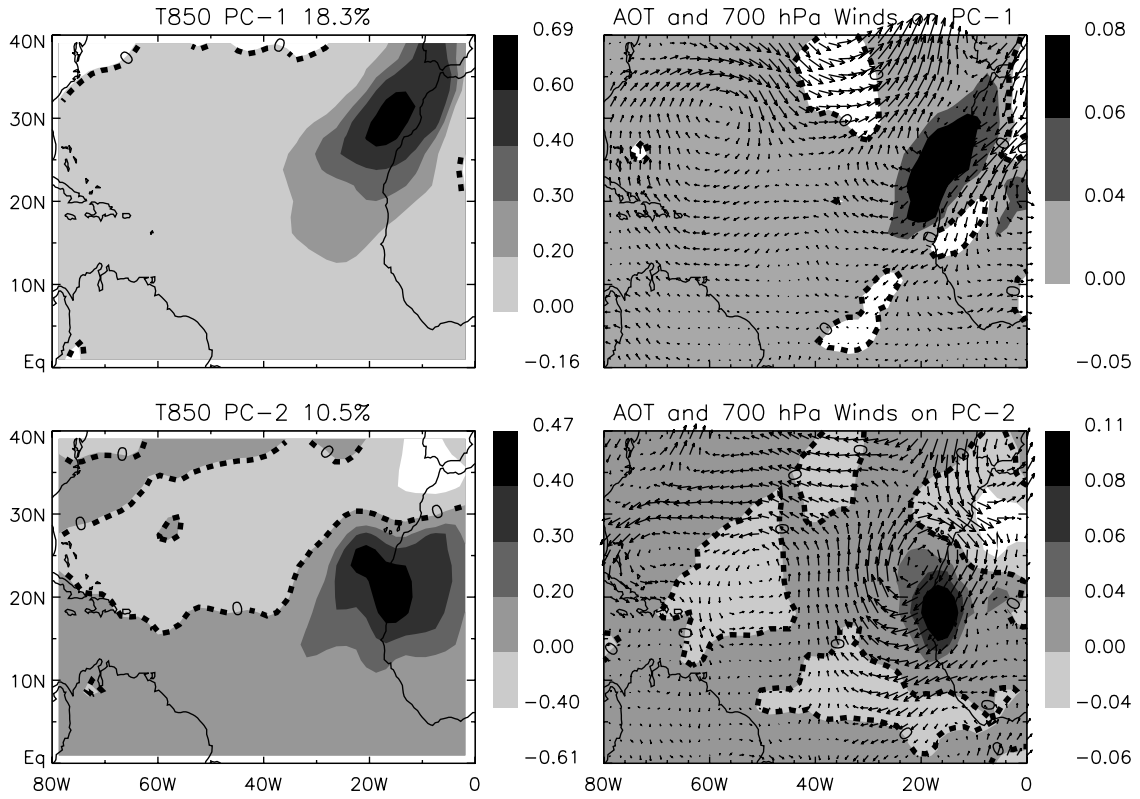

Figure 2. (left) Geographical distributions of the first two empirical orthogonal functions (units in K) of the variation of 850 hPa NCEP reanalysis temperature anomalies for June–September 2002 over 0–40°N and 0–80°W. (right) CARMA dust AOT (at 0.55 μm) and the NCEP wind anomalies at 700 hPa projected onto the time series of the (top) first and (bottom) second PCs.

following, we will utilize the time series of the first PC (Figure 1, top) as an index to indicate the timing of the beginning of SAL episodes at the west coast of Africa. We define the onset of SAL episodes as when the index exceeds the value of one (meaning that the warm anomalies are more than the 1σ-confidence level).

[15] The second EOF (EOF-2, Figure 2, bottom left) shows a dipole pattern. One end of the dipole (positive values) is located at the west coast of Africa between about 15°N and 30°N, at the south of the maximum seen in EOF-1. The other end of the dipole (negative values) is located northward of 30°N over the northwest African coast and southwest Europe. The small values of the EOFs in the West Atlantic Ocean are subjected to interannual variability. The regression of dust AOT anomalies on the second PC also shows a similar dipole pattern (Figure 2, bottom right) with the centers located slightly southward of the centers of the temperature anomalies. The second PC represents two different directions for SAL migrations during June–September 2002. We utilize the time series of the second PC (Figure 1, bottom) as an index to define the direction of migration of the SAL. The positive phase, when the index has positive values, corresponds to the southward and westward migration of the SAL into the tropical-subtropical North Atlantic Ocean; the negative phase corresponds to the northward migration of the SAL into the subtropical to midlatitude North Atlantic Ocean and southwest Europe. The evolution of the SAL in the positive phase is similar to the propagation of the SAL related dry air outbreaks described by *Zhang and Pennington* [2004].

[16] The SAL's two different migration pathways are related to the anomaly wind pattern off the west coast of Africa. For the positive phase (Figure 2, bottom right), the northeasterly anomaly winds at the east and south boundaries of the warm anomalies around 15–20°N strengthen the easterly trade winds transporting dust westward. For the negative phase, the direction of anomaly winds reverses and becomes onshore, weakening the offshore transport of dust at 10–20°N into the Atlantic Ocean. Instead, more dust tends to be advected northward to northwest Africa and southwest Europe.

[17] In conclusion, the migration of SAL from the African continent is correlated with the variation of the offshore winds at about 10–20°N over the west coast of North Africa. Previous studies also found high correlations between dust AOT and westward winds off the west coast of North Africa at the same latitudes [*Karyampudi and Carlson*, 1988; *Kaufman et al.*, 2005].

3.2. Temporal Evolution

[18] We pick from Figure 1 four individual SAL outbreaks, starting on 10 June (episode 1), 21 June (episode 2), 23 July (episode 3), and 5 September (episode 4). All four episodes have the values of the first PC index greater than one (meaning that the warm anomalies are more than 1-σ confidence level at the onset). We examine the evolution of each episode by computing the time lag composites of the temperature and dust AOT anomalies. The time lag composites are 4-day averages of the anomalies with time lags from the onset dates. For example, for episode 4 the zero-day lag

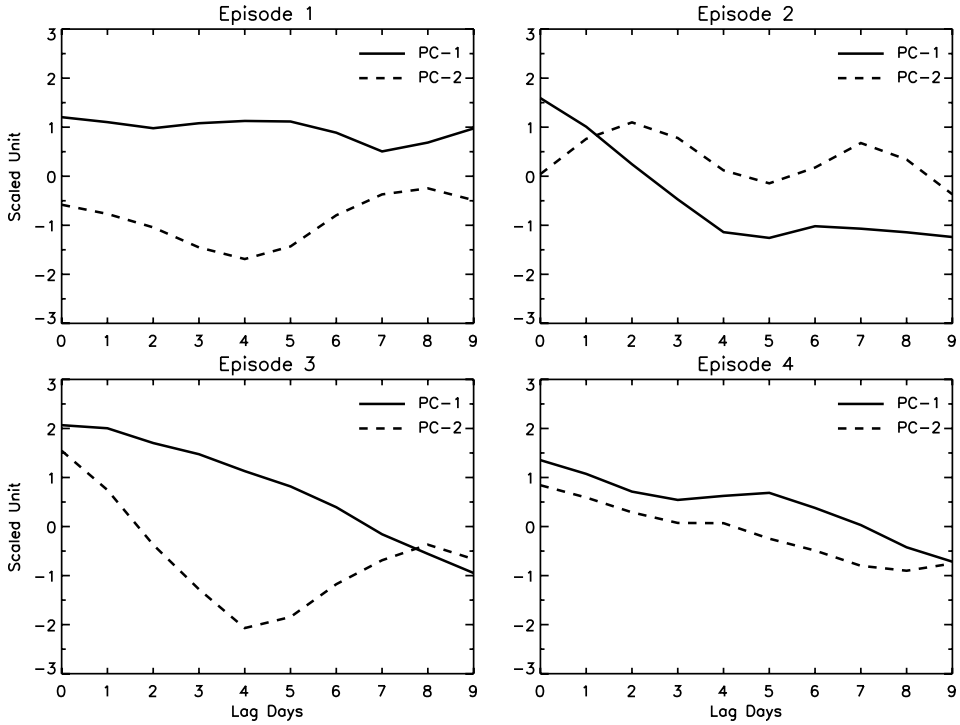

Figure 3. Time lag evolutions of the 4-day averages of the first (solid lines) and second (dashed lines) PC time series, starting from the onset dates of the four main warm episodes occurring in June–September 2002. The ordinates are scaled by the standard deviations of the time series.

composite is the 4-day averages of the anomalies from 5 to 8 September, the 2-day lag composite is the 4-day averages from 7 to 9 September, and so on. The composites allow us to compare the results from reanalysis temperatures and CARMA AOT with those from satellite data, because missing values in the satellite observations because of cloud contamination or orbital gaps are mostly filled in by the 4-day averaging of the data.

[19] Since the temperature anomalies on each day can be expanded by the PCs, we can use the time series of the first two PCs to give an overview of the evolution of the warm anomalies near the west coast of Africa. Let $T(x, t_i)$ be the temperature anomalies at position x on day t_i, the 4-day averages of the anomalies starting on the day t_i can be expressed as

$$\overline{T}(x,t_i) = \frac{1}{4}\sum_{n=0}^{3} T(x,t_i+n) = \frac{1}{4}\sum_{n=0}^{3}\sum_{m} c_m(t_i+n)\cdot\psi_m(x)$$
$$= \sum_{m}\left(\frac{1}{4}\sum_{n=0}^{3} c_m(t_i+n)\right)\cdot\psi_m(x)$$

where $c_m(t)$ represents the time series for the mth PC and $\psi_m(x)$ represents the mth EOF. Therefore the time lag composites of the PC time series, $\frac{1}{4}\sum_{n=0}^{3} c_m(t_i+n)$, provide a means to investigate the evolution of each episode. Figure 3 shows the time lag composites of the first two PC time series (i.e., $\frac{1}{4}\sum_{n=0}^{3} c_m(t_i+n)$, for $m = 1, 2$), beginning on the individual onset dates of the four main episodes. Episode 1 has relatively flat time lag variation of the composites of the first PC time series, because of the several successive events after the first episode (e.g., events from 13 to 15 June, see Figure 1, top). The time lag composites of the second PC time series are mainly negative for episode 1, meaning that the anomaly winds near the west coast of Africa were blowing onshore, and were mainly positive for episode 2, meaning that the anomaly winds were blowing offshore.

[20] Figure 4 shows the corresponding spatial distributions of the temperature anomalies and CARMA dust AOT anomalies for the 2-day lag composites of episodes 1 and 2. The distributions of the warm anomalies of these two episodes (Figure 4, left) are consistent with the EOF-2 pattern (Figure 2, bottom left). The negative-phase-dominated episode 1 has the warm anomalies distributed primarily north of 20°N, over the subtropical to midlatitude Atlantic Ocean. The positive-phase-dominated episode 2 has the warm anomalies extending southwestward into the tropical North Atlantic Ocean. In episode 1, the transport of dust westward at 15–20°N is suppressed by the onshore wind anomalies at the west coast of Africa. Consequently, more dust tends to travel northward to Europe, and some heads southwestward into the deep tropical Atlantic Ocean (Figure 4, top right). In contrast, during episode 2, the dust is transported into the Atlantic Ocean around 15–30°N by the offshore wind anomalies (Figure 4, bottom right).

[21] For episode 3, the time lag composite of the second PC time series (Figure 3, bottom left) changes sign around the second day after the onset, implying that there is a change in the near-coast wind direction, accordingly altering the evolution of the warm anomaly. For episode 4, the averaged second PC time series remains positive for about 4 days after the onset. For this period, the offshore anomaly winds near the west coast of North Africa drive the evolution of the SAL and dust transport. On the 5th to 6th day after the onset, the phase becomes negative and onshore anomaly winds

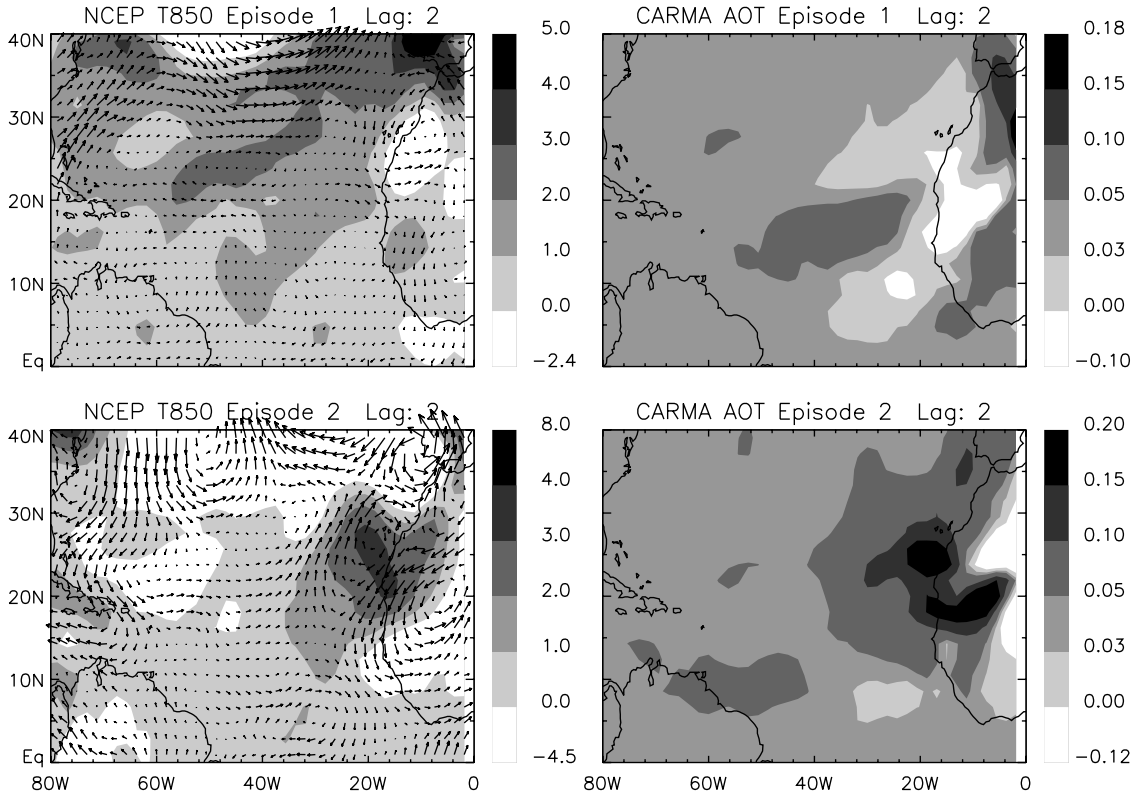

Figure 4. Second-day lag composites (left) of the 850-hPa NCEP temperature anomalies (in K) and 700-hPa wind anomalies and (right) of the CARMA dust AOT. (top) Composites for episode 1 and (bottom) composites for episode 2.

dominate. In the next three subsections, we will focus on episodes 3 and 4 and compare the reanalysis and model results with satellite retrievals.

3.3. Evolution of Episode 3

[22] Figure 5 illustrates the evolution of the warm anomalies associated with the SAL for episode 3 (onset day on 23 July). Figure 5 also shows the composites of wind anomalies associated with the warm anomalies on each day lag. The corresponding CARMA and MODIS dust AOT composites are shown in Figures 6 and 7.

[23] The composite on the 0-day lag (23–26 July) shows that the 850-hPa warm anomalies extend southwest toward the tropical Atlantic Ocean (Figure 5, top left). The corresponding composite of the second PC time series (Figure 3, bottom left) is positive and the distribution of the warm anomalies is consistent with the positive-phase of the second PC. Over the eastern North Atlantic Ocean near the west coast of Africa, offshore wind anomalies located south of the warm anomalies are responsible for blowing the dust off the west coast of Africa; hence the dust AOT maximum is located slightly south of the warm anomalies. However, the simulated dust AOT anomalies (Figure 6, top left) extend more westward than the warm anomalies. The MODIS AOT measurements (Figure 7, top left) confirm the distribution of the CARMA dust AOT, although the simulated dust AOT anomalies are lower than the MODIS retrieved values. The difference between the MODIS and CARMA AOT is larger than the expected factor of 2 mentioned in the section of satellite data (see section 2.2), probably because of overestimation of dust removal in CARMA. In this study, however, the main focus is to examine the patterns of dust distribution and not the specific magnitudes of AOT. Differences between MODIS and CARMA AOT values do not affect our main conclusions. The incoherence in the spatial distribution of the warm anomalies and the dust AOT anomalies in the western North Atlantic Ocean may be attributed to the limitation of using the 850 hPa temperature to track the SAL in the West Atlantic Ocean.

[24] As the phase of the second PC changes from positive to negative after day 2 from the onset (Figure 3, bottom left), the warm anomalies on the west coast of North Africa are pushed northward by a strengthening cyclonic circulation located south of the warm anomalies near the west coast of Africa around 20°N (Figure 5, top right). The transport of dust is accordingly altered by the changed circulation. On the fourth- to sixth-day lag, the wind anomalies near the west coast of North Africa around 20°N blow onshore, and the dust follows the circulation pattern and is distributed northward over the northwest coast of Africa into the midlatitude Atlantic Ocean (Figures 5 and 6, bottom left). The corresponding MODIS AOT images (Figure 7, top right and bottom) also capture the northward transport of dust.

3.4. Evolution of Episode 4

[25] Figure 8 shows the evolution of the warm anomalies of episode 4 (onset on 5 September) and the associated anomaly wind composites. We also compare in Figure 9 the evolution of this episode with that seen in AIRS retrieved

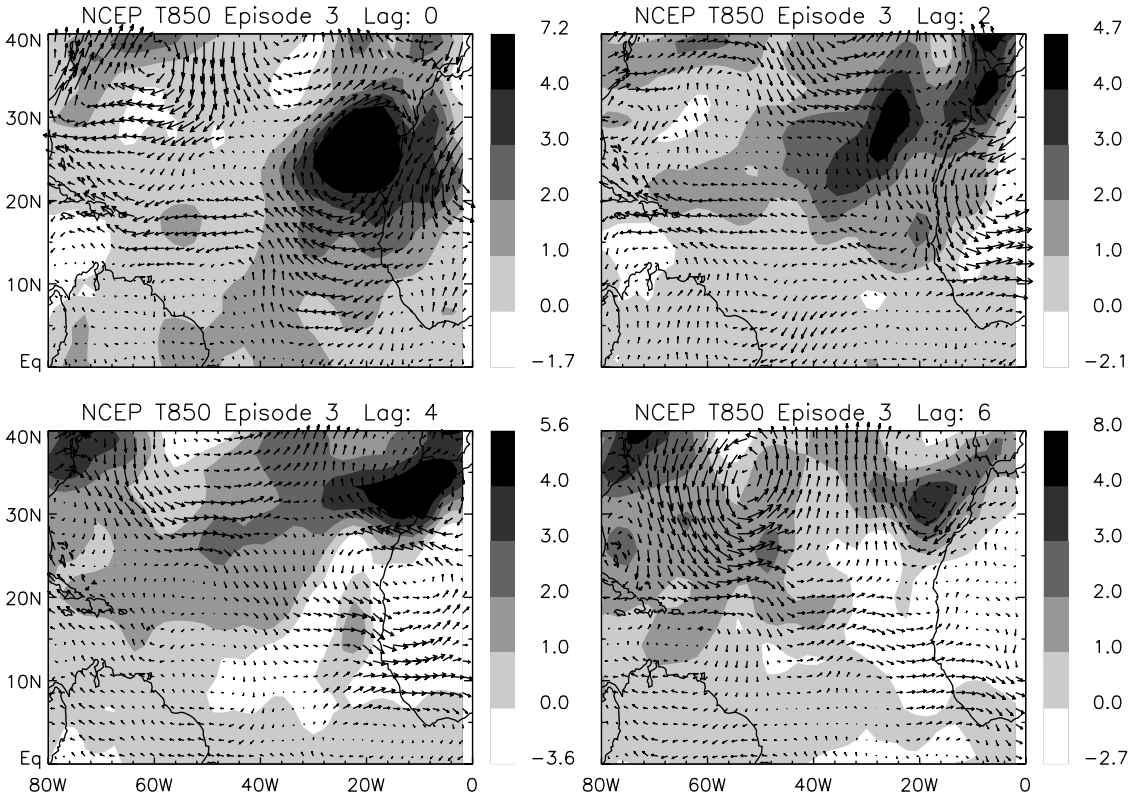

Figure 5. Time lag composites of the 850-hPa NCEP temperature anomalies (in K) and 700-hPa wind anomalies for episode 3. The zero-, second-, fourth-, and sixth-day lag composites are shown.

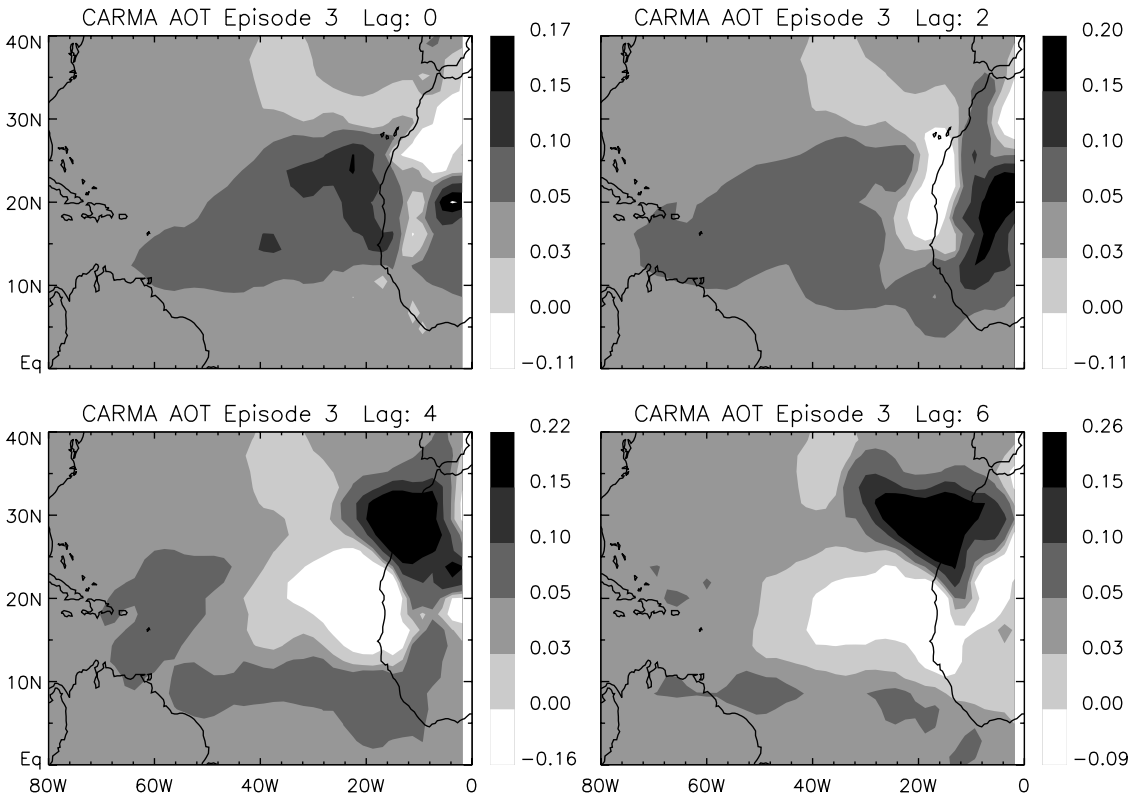

Figure 6. Time lag composites of the CARMA dust AOT computed at 0.55μm for episode 3. The zero-, second-, fourth-, and sixth-day lag composites are shown.

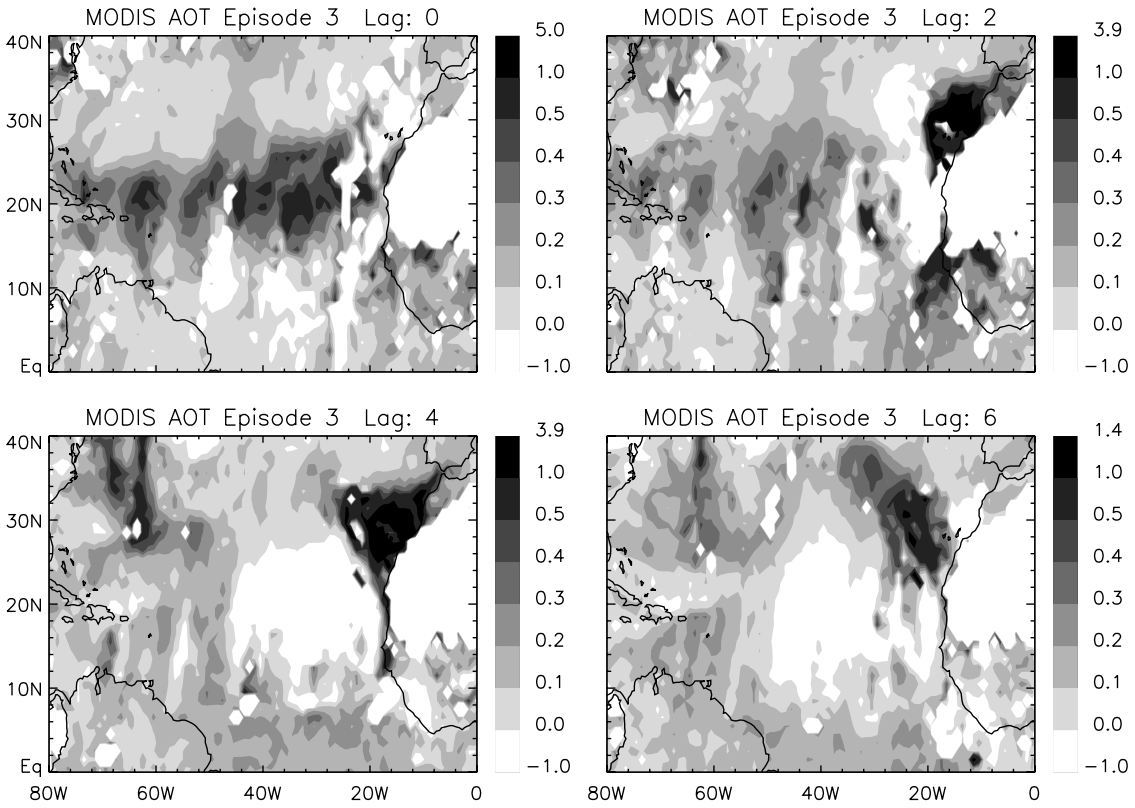

Figure 7. Similar to Figure 6 but for MODIS AOT at 0.55 μm. Missing data are set as negative and in white.

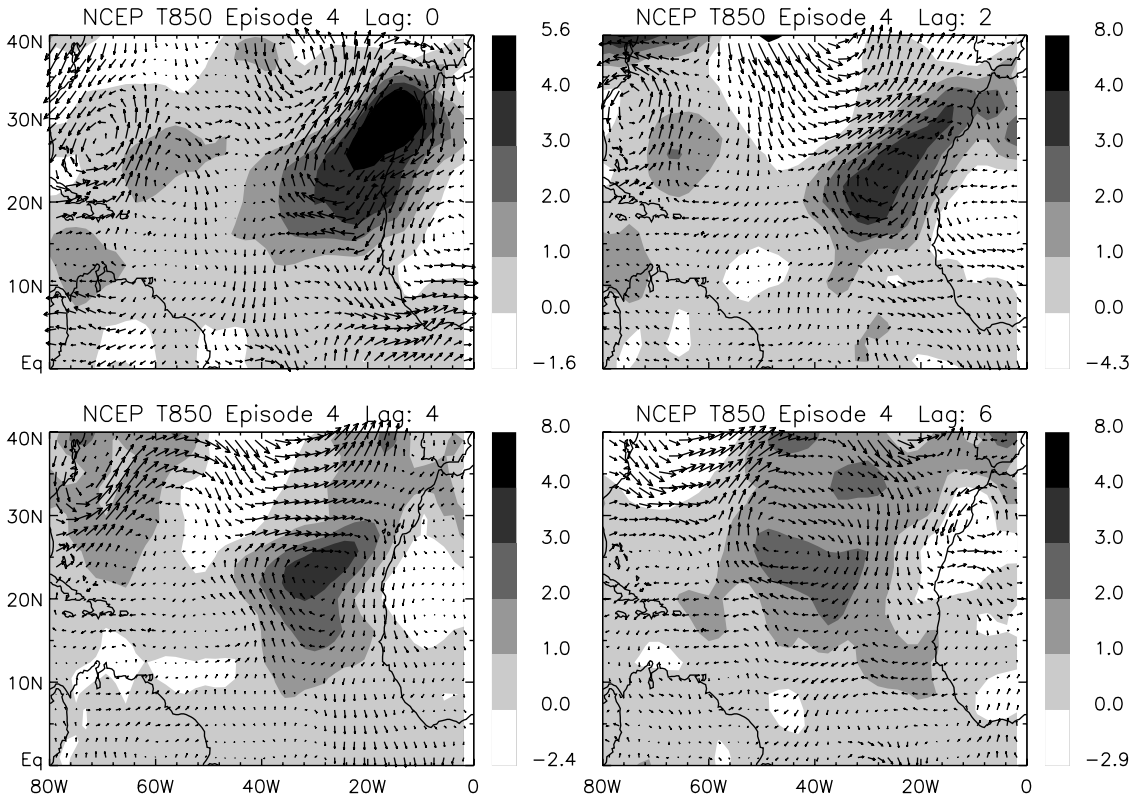

Figure 8. Similar to Figure 5 but for episode 4.

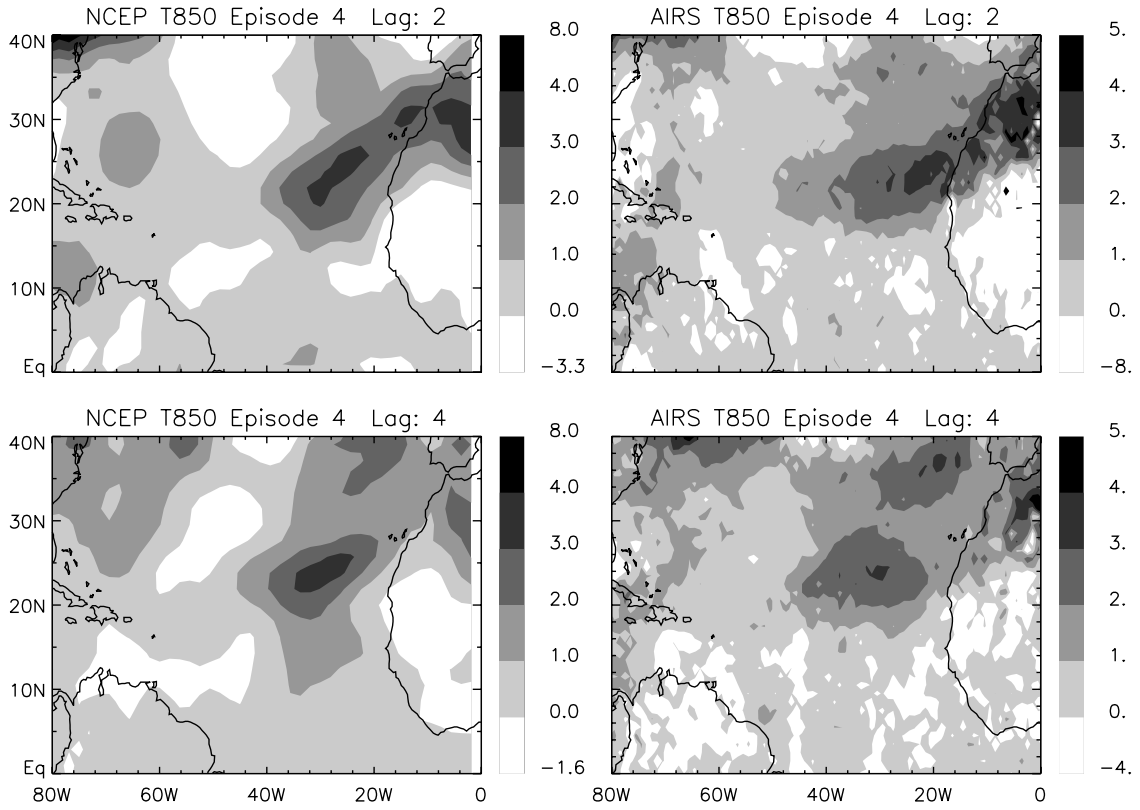

Figure 9. Comparisons of time lag composites computed from the 850-hPa NCEP temperature anomalies and the 850-hPa AIRS temperature anomalies (units in K) for episode 4. The anomalies are computed as the difference of the temperature fields and the September mean. (top) Results for the second-day lag composites and (bottom) results for the fourth-day lag composites.

temperatures for the second- and fourth-day lags. Since we have only AIRS data for September in 2002, we obtain the warm anomalies in Figure 9 by subtracting the monthly mean temperatures of September 2002, instead of the averages of the 15-day period before and after the onset day. Comparing the lag 2 and lag 4 plots of Figure 9 with the corresponding plots of Figure 8, we can see that the various methods of determining the anomaly field produce similar results. Figure 9 shows that the warm anomalies depicted by the NCEP reanalysis temperatures are remarkably consistent with the retrieved temperatures from the AIRS instrument.

[26] In this episode, the phase of the second PC is positive when the warm anomalies are in the East Atlantic Ocean, and the warm anomalies move westward at a latitude of about 20–30°N (Figures 8 and 9). The associated CARMA and MODIS dust AOT anomalies are shown in Figures 10 and 11, respectively. Again, the offshore wind anomalies at the southern boundary of the warm anomalies (Figure 8, top) blow the dust off the west coast of Africa, and the dust moves westward into the tropical-subtropical North Atlantic Ocean. In the East and Central Atlantic Ocean, the dust is transported by the anticyclonic jet circulating the warm anomalies and located slightly off the center of the warm anomalies, consistent with a long-term simulation performed by *Jones et al.* [2004, Figures 1 and 2]. CARMA can reproduce the westward transport of dust (Figure 10) as seen in the MODIS measurements (Figure 11), although detailed differences in dust distributions between CARMA and MODIS become more evident in later time lag composites.

3.5. Distribution of Dust Deposition

[27] We have argued that the distribution of the deposition of dust over the eastern tropical North Atlantic Ocean and the northwest Africa to southwest Europe is dependent on the phase of the second PC. To quantify this, we compute the distribution of dust deposition between two regions using the CARMA simulated dust deposition, which is the sum of dry deposition and scavenging in large-scale and convective clouds. The first region covers the eastern tropical North Atlantic Ocean (20–40°W and 0–30°N). The second region covers the area from northwest Africa to southwest Europe (0–20°W and 30–45°N).

[28] Table 1 shows the relative distribution of dust deposition between the two regions for four SAL episodes from June–September 2002. Because of the change of phase in the second PC during episode 3, we average the dust deposition for the first 4 days (day 0 to 3) and the successive 4 days (day 4 to 7) from the onset dates of each episode. The relative distributions are shown in percentage of the combined dust deposition in the two regions for each averaged period in each episode. Also shown in Table 1 are the combined dust depositions of the two regions and the averaged second PC values for the averaging period.

[29] In episode 1, the second PC is mainly in the negative phase and relatively more dust is deposited into northwest Africa and southwest Europe (Table 1). Episode 2 is mainly

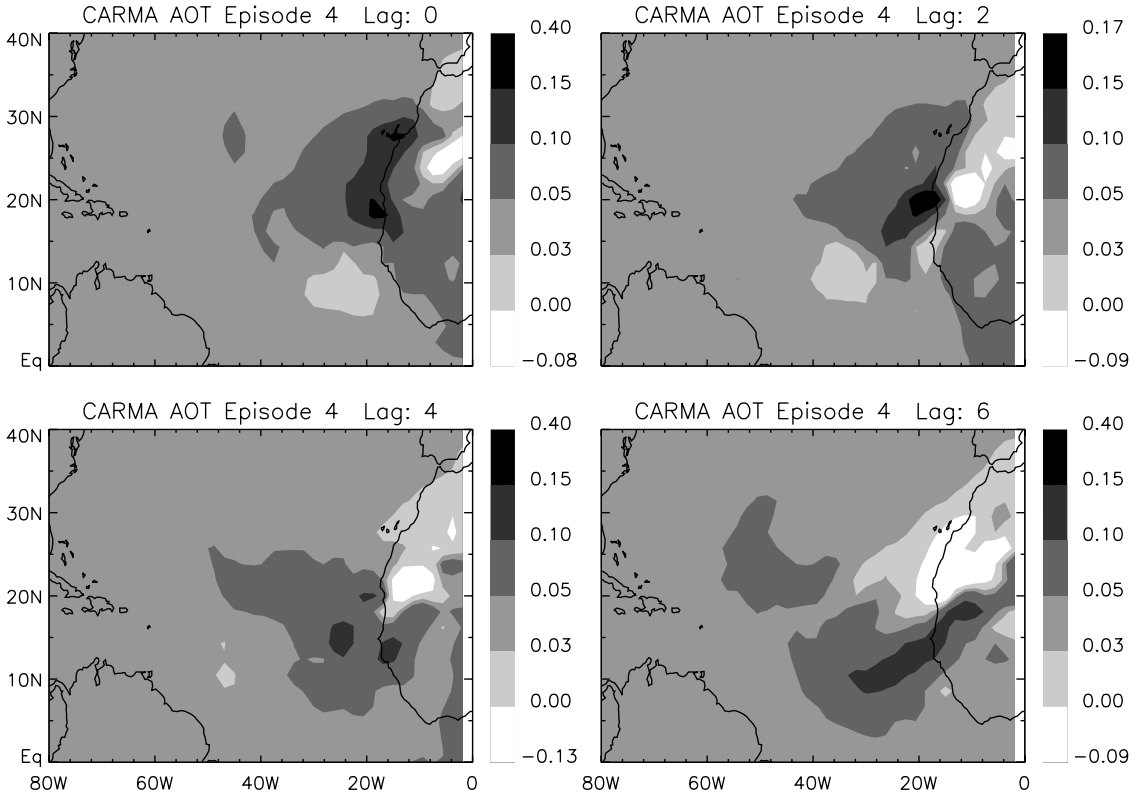

Figure 10. Similar to Figure 6 but for episode 4.

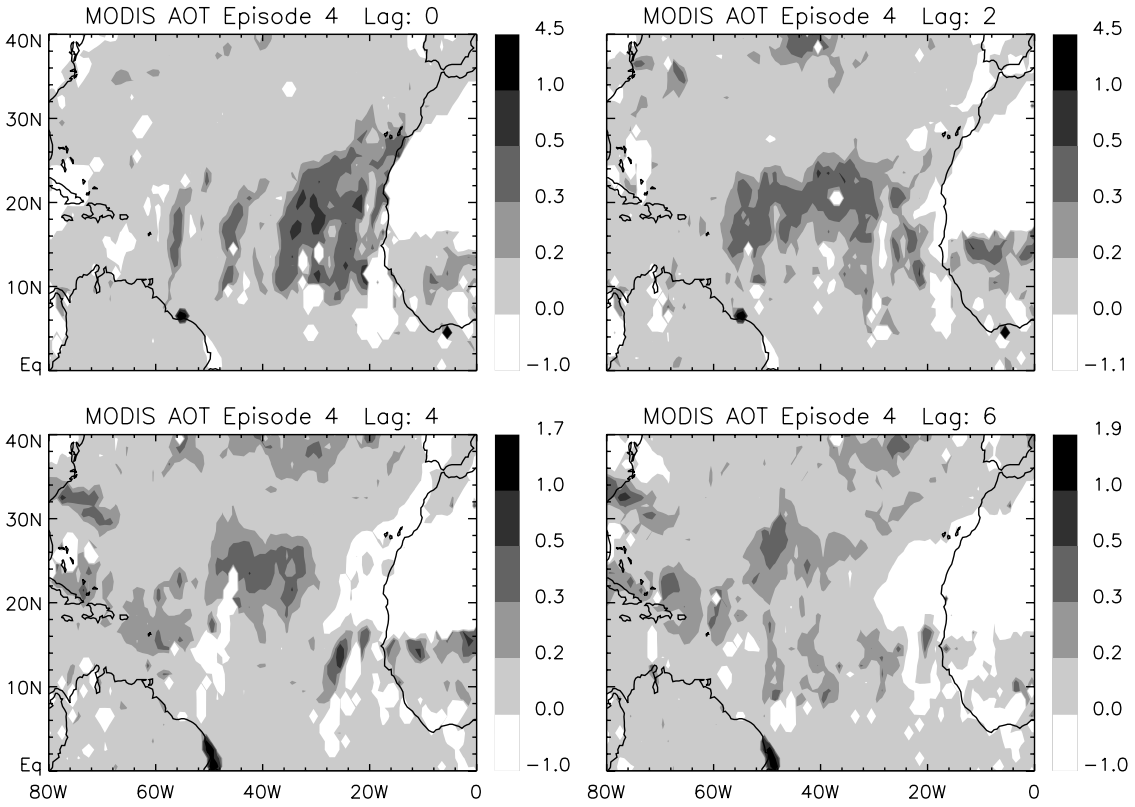

Figure 11. Similar to Figure 7 but for episode 4.

Table 1. CARMA Dust Deposition Over the Eastern Tropical North Atlantic Ocean (20–40°W and 0–30°N) and Northwest Africa and Southwest Europe (0–20°W and 30–45°N) for the Four SAL Episodes in June–September 2002[a]

Episode	Total Deposition, Tg	Eastern Atlantic, %	Northwest Africa and Southwest Europe, %	Averaged 2nd-PC Index
1	0.18	34	66	−0.58
1	0.19	27	73	−1.69
2	0.19	61	39	0.04
2	0.31	53	47	0.12
3	0.24	85	15	1.55
3	0.21	50	50	−2.07
4	0.27	94	6	0.84
4	0.19	95	5	0.07

[a]The first row in each episode is the average of dust deposition for the first 4 days (day 0 to 3) of the episode; the second row is the average over the next 4 days (day 4 to 7). Relative distributions over each region are also shown in percentage. The 4-day averaged second-PC indices (see text) for each period are shown in the last column.

in the positive phase of the second PC and has more dust deposited over the eastern tropical Atlantic Ocean. In episode 3, the phase of the second PC changes from positive to negative around the second-day lag (Figure 3, bottom left). The first 4-day average for episode 3 in Table 1 shows dust deposition distributed mainly over the eastern tropical Atlantic Ocean (85% versus 15%); however, the second 4-day average shows an increased portion of dust deposition distributed over the northwest Africa and southwest Europe (50% versus 50%). The second PC for episode 4 does not change its sign until the fourth-day lag (Figure 3, bottom right), when most dust associated with the warm anomalies has already migrated into the central North Atlantic Ocean. Therefore a large portion of dust deposition is distributed over the eastern tropical Atlantic Ocean.

[30] In conclusion, there are at least two transport pathways for North African dust. The first is directly westward into the tropical to subtropical Atlantic, while a second is northwestward toward midlatitude Atlantic and Europe. The second PC of the temperature anomaly gives us a measure of the importance at any given time of this pathway: relatively more (less) dust is deposited over northwest Africa and southwest Europe than over the eastern tropical North Atlantic Ocean, if the second PC has negative (positive) phase.

4. Conclusions and Discussion

[31] Principal component (PC) analysis is applied to NCEP temperature anomalies at 850 hPa for June–September 2002. The first PC can be used to determine the onset of SAL episodes, which are associated with large warm anomalies located just off the west coast of North Africa. The second PC has a dipole pattern that represents opposite phases of the evolution of the SAL. In the positive phase, the SAL tends to migrate southwestward into the subtropical to tropical Atlantic Ocean. In the negative phase, the SAL tends to migrate into the subtropical to midlatitude North Atlantic Ocean, northwest Africa and southwest Europe. The phase of the second PC is related to the direction of wind anomalies at 700 hPa near the west coast of North Africa around 10–20°N. In its positive phase, the 700 hPa wind anomalies are associated with stronger offshore flow. In the negative phase, the anomaly circulation pattern reverses and the offshore flow near the west coast of North Africa around 10–20°N is weakened.

[32] The NCEP reanalysis wind fields are used to drive CARMA to simulate the corresponding dust distribution and deposition. The dust AOT anomalies simulated by CARMA have patterns in agreement with those seen in MODIS AOT anomalies, although CARMA underestimates the total AOT. Compared with the AIRS temperature retrievals in September 2002, NCEP temperatures at 850 hPa reproduce the migration of the warm anomalies associated with the SAL of our episode 4.

[33] There are at least two transport pathways for North African dust. The first is directly westward into the tropical to subtropical Atlantic, while a second is northwestward toward midlatitude Atlantic and southwest Europe. The second PC of the temperature anomaly gives us a measure of the importance at any given time of this pathway: relatively more (less) dust is deposited over northwest Africa and southwest Europe than over the eastern tropical North Atlantic Ocean, if the second PC has negative (positive) phase. Dust is transported out of the African continent by the offshore midlevel jet (at about the 700-hPa level) associated with the anticyclone generated by the warm anomalies. This implies that the midlevel jet plays a role in connecting the dust with the warm anomalies, while earlier studies have demonstrated the important role of the absorption of infrared radiation by dust [*Alpert et al.*, 1998; *Stephens et al.*, 2004; *Weaver et al.*, 2003].

[34] There are limitations to this study and we discuss them in the following. It is clear from studies of simple models that heating from dust can alter the circulation pattern of the atmosphere [*Stephens et al.*, 2004]. *Alpert et al.* [1998] and *Jones et al.* [2004] compared the spatial distributions of assimilation increments in temperatures and of dust and suggested that dust has a warming effect at least over the eastern tropical North Atlantic Ocean. The correlation between the temperature increments and the dust concentrations vanish in the central to western North Atlantic Ocean, possibly because of the relatively sparse measurements for computing the assimilation increments. However, *Weaver et al.* [2002, 2003] pointed out that such correlation between assimilation increments and dust concentrations can also be caused by a bias in the satellite retrievals of temperatures used to feed the data assimilation. Contamination of temperature retrievals from infrared sounder may exist over regions of high dust concentrations, if absorption of infrared radiation by dust is not accounted for in the retrieval algorithms [*Weaver et al.*, 2003]. Such contamination exists in NCEP reanalysis temperatures and may also exist in AIRS temperature retrievals. Therefore the estimated magnitudes of 850 hPa temperature anomalies, in particular over the region of East Atlantic Ocean near the west coast of North Africa, may contain biases. Identification of such errors requires a retrieval algorithm that accounts for the absorption of infrared radiation by dust and future work on this issue is outside the scope of this paper.

[35] We have identified that the evolution of several 2002 SAL outbreaks described by the second PC was associated with the strengthening of the easterlies at 700 hPa around 10–20°N, because of the enhanced meridional temperature gradient at 850 hPa. Several studies [e.g., *Carlson and*

Prospero, 1972; *Cook*, 1999; *Dunion and Velden*, 2004] have indicated or implied the relation between the SAL and the African easterly jet, a component of the West African Monsoon [*Fontaine et al.*, 1995; *Moron et al.*, 2004; *Palmer et al.*, 1992]. It will be interesting to further investigate the relationship among the evolution of the SAL, the subseasonal variation of the West African Monsoon, and the African Easterly Wave with data sets of longer timescale.

[36] Finally, we have studied only the warm anomalies and dust associated with the SAL. Because of the quality of water vapor data in both satellite retrievals and NCEP reanalysis, we do not include the analysis of the humidity anomalies associated with the SAL. Since the dryness of the SAL is also important for influencing the development of TCs [*Dunion and Velden*, 2004; *Zhang and Pennington*, 2004], it will be an urge to repeat this analysis on humidity anomalies once the quality of water vapor data are improved.

[37] **Acknowledgments.** We thank Gerald North and Ramalingam Saravanan for helpful discussions of the analysis method. We also thank Alexander Dessler, Natalie Mahowald of NCAR, Alf Grini of University of Oslo and three anonymous reviewers for their comments. We acknowledge the NASA/GSFC MODIS atmospheres group and NASA/JPL AIRS science team for their high-quality level-3 products. This work was supported by NASA EOS/IDS grant NNG04GH67G to Texas A&M University.

References

Ackerman, A., O. B. Toon, and P. V. Hobbs (1995), A model for particle microphysics, turbulent mixing, and radiative transfer in the stratocumulus-topped marine boundary layer and comparisons with measurements, *J. Atmos. Sci.*, *52*, 1204–1236.

Alpert, P., Y. J. Kaufman, Y. Shay-El, D. Tanré, A. da Silva, S. Schubert, and J. H. Joseph (1998), Quantification of dust-forced heating of the lower troposphere, *Nature*, *395*, 367–370.

Balkanski, Y. J., D. J. Jacob, G. M. Gardner, W. C. Graustein, and K. K. Turekian (1993), Transport and residence times of tropospheric aerosols inferred from a global three-dimensional simulation of ^{210}Pb, *J. Geophys. Res.*, *98*, 20,573–20,586.

Bretherton, C. S., C. Smith, and J. M. Wallace (1992), An intercomparison of methods for finding coupled patterns in climate data, *J. Clim.*, *5*, 541–560.

Carlson, T. N., and J. M. Prospero (1972), The large-scale movement of Saharan air outbreaks over the northern equatorial Atlantic, *J. Appl. Meteorol.*, *11*, 283–297.

Colarco, P. R., O. B. Toon, and B. N. Holben (2003), Saharan dust transport to the Caribbean during PRIDE: 1. Influence of dust sources and removal mechanisms on the timing and magnitude of downwind aerosol optical depth events from simulations of in situ and remote sensing observations, *J. Geophys. Res.*, *108*(D19), 8589, doi:10.1029/2002JD002658.

Cook, K. H. (1999), Generation of the African Easterly Jet and its role in determining west African precipitation, *J. Clim.*, *12*, 1165–1184.

Divakarla, M. G., C. D. Barnet, M. D. Goldberg, L. M. McMillin, E. Maddy, W. Wolf, L. Zhou, and X. Liu (2006), Validation of Atmospheric Infrared Sounder temperature and water vapor retrievals with matched radiosonde measurements and forecasts, *J. Geophys. Res.*, *111*, D09S15, doi:10.1029/2005JD006116.

Dunion, J. P., and C. S. Velden (2004), The impact of the Saharan air layer on Atlantic tropical cyclone activity, *Bull. Am. Meteorol. Soc.*, *85*, 353–365.

Fontaine, B., S. Janicot, and V. Moron (1995), Rainfall anomaly patterns and wind field signals over West Africa in August (1958–1989), *J. Clim.*, *8*, 1503–1510.

Ginoux, P., M. Chin, I. Tegen, J. M. Prospero, B. Holben, O. Dubovik, and S.-J. Lin (2001), Sources and distributions of dust aerosols simulated with the GOCART model, *J. Geophys. Res.*, *106*(D17), 20,255–20,273.

Jones, C., N. Mahowald, and C. Luo (2004), Observational evidence of African desert dust intensification of easterly waves, *Geophys. Res. Lett.*, *31*, L17208, doi:10.1029/2004GL020107.

Kalnay, E., et al. (1996), The NCEP/NCAR 40-year reanalysis project, *Bull. Am. Meteorol. Soc.*, *77*, 437–471.

Karyampudi, V. M., and T. N. Carlson (1988), Analysis and numerical simulations of the Saharan air layer and its effect on easterly wave disturbances, *J. Atmos. Sci.*, *45*, 3103–3136.

Karyampudi, V. M., et al. (1999), Validation of the Saharan dust plume conceptual model using lidar, Meteosat, and ECMWF data, *Bull. Am. Meteorol. Soc.*, *80*, 1045–1075.

Kaufman, Y. J., D. Tanré, L. A. Remer, E. Vermote, A. Chu, and B. N. Nolben (1997), Operational remote sensing of tropospheric aerosol over land from EOS moderate resolution imaging spectroradiometer, *J. Geophys. Res.*, *102*, 17,051–17,067.

Kaufman, Y. J., I. Koren, L. A. Remer, D. Tanré, P. Ginoux, and S. Fan (2005), Dust transport and deposition observed from the Terra-Moderate Resolution Imaging Spectroradiometer (MODIS) spacecraft over the Atlantic Ocean, *J. Geophys. Res.*, *110*, D10S12, doi:10.1029/2003JD004436.

King, M. D., W. P. Menzel, Y. J. Kaufman, D. Tanré, B.-C. Gao, S. Platnick, S. A. Ackerman, L. A. Remer, R. Pincus, and P. A. Hubanks (2003), Cloud and aerosol properties, precipitable water, and profiles of temperature and water vapor from MODIS, *IEEE Trans. Geosci. Remote Sens.*, *41*, 442–458.

Levy, R. C., L. A. Remer, D. Tanré, Y. J. Kaufman, C. Ichoku, B. N. Holben, J. M. Livingston, P. B. Russell, and H. Maring (2003), Evaluation of the Moderate-Resolution Imaging Spectroradiometer (MODIS) retrievals of dust aerosol over the ocean during PRIDE, *J. Geophys. Res.*, *108*(D19), 8594, doi:10.1029/2002JD002460.

Mahowald, N., C. Luo, J. del Corral, and C. S. Zender (2003), Interannual variability in atmospheric mineral aerosols from a 22-year model simulation and observational data, *J. Geophys. Res.*, *108*(D12), 4352, doi:10.1029/2002JD002821.

Moron, V., N. Philippon, and B. Fontaine (2004), Simulation of West African monsoon circulation in four atmospheric general circulation models forced by prescribed sea surface temperature, *J. Geophys. Res.*, *109*, D24105, doi:10.1029/2004JD004760.

North, G. R., T. L. Bell, R. F. Cahalan, and F. J. Moeng (1982), Sampling errors in the estimation of empirical orthogonal functions, *Mon. Weather Rev.*, *110*, 699–706.

Palmer, T. N., C. Brankovice, P. Viterbo, and M. J. Miller (1992), Modeling inter-annual variations of summer monsoons, *J. Clim.*, *5*, 399–417.

Prospero, J. M., and T. N. Carlson (1972), Vertical and area distributions of Saharan dust over the western equatorial North Atlantic Ocean, *J. Geophys. Res.*, *77*, 5255–5265.

Rasch, P. J., N. M. Mahowald, and B. E. Eaton (1997), Representations of transport, convection, and hydrologic cycle in chemical transport models: Implications for the modeling short-lived and soluble species, *J. Geophys. Res.*, *102*(D23), 28,127–28,138.

Remer, L. A., et al. (2002), Validation of MODIS aerosol retrieval over ocean, *Geophys. Res. Lett.*, *29*(12), 8008, doi:10.1029/2001GL013204.

Stephens, G. L., N. B. Wood, and L. A. Pakula (2004), On the radiative effects of dust on tropical convection, *Geophys. Res. Lett.*, *31*, L23112, doi:10.1029/2004GL021342.

Strow, L. L., S. E. Hannon, S. De Souza-Machado, H. E. Motteler, and D. Tobin (2003), An overview of the AIRS radiative transfer model, *IEEE Trans. Geosci. Remote Sens.*, *41*, 303–313.

Susskind, J., C. Barnet, and J. Blaisdell (1998), Determination of atmospheric and surface parameters from simulated AIRS/AMSU/HSB/ sounding data: Retrieval and cloud clearing methodology, *Adv. Space Res.*, *21*(3), 369–384.

Tegen, I., and R. Miller (1998), A general circulation model study on the interannual variability of soil dust aerosol, *J. Geophys. Res.*, *103*(D20), 25,975–25,995.

Toon, O. B., R. P. Turco, D. Westphal, R. Malone, and M. S. Liu (1988), A multidimensional model for aerosols: Description of computational analogs, *J. Atmos. Sci.*, *45*(15), 2123–2143.

Weaver, C. J., P. Ginoux, N. C. Hsu, M.-D. Chou, and J. Joiner (2002), Radiative forcing of Saharan dust: GOCART model simulations compared with ERBE data, *J. Atmos. Sci.*, *59*, 736–747.

Weaver, C. J., J. Joiner, and P. Ginoux (2003), Mineral aerosol contamination of TIROS Operational Vertical Sounder (TOVS) temperature and moisture retrievals, *J. Geophys. Res.*, *108*(D8), 4246, doi:10.1029/2002JD002571.

Wong, S., and A. E. Dessler (2005), Suppression of deep convection over the tropical North Atlantic by the Saharan air layer, *Geophys. Res. Lett.*, *32*, L09808, doi:10.1029/2004GL022295.

Wong, S., and W.-C. Wang (2003), Tropical-extratropical connection in interannual variation of the tropopause: Comparison between NCEP/NCAR reanalysis and an atmospheric general circulation model simulation, *J. Geophys. Res.*, *108*(D2), 4043, doi:10.1029/2001JD002016.

Zhang, C., and J. Pennington (2004), African dry air outbreaks, *J. Geophys. Res.*, *109*, D20108, doi:10.1029/2003JD003978.

P. R. Colarco, NASA Goddard Space Flight Center, Greenbelt, MD 20771, USA.

A. E. Dessler and S. Wong, Department of Atmospheric Science, Texas A&M University, College Station, TX 77843, USA. (swong@ariel.met.tamu.edu)